A Two-Photon Excitation Fluorescence Cross-Correlation Assay for a Model Ligand-Receptor Binding System Using Quantum Dots

J. L. Swift, R. Heuff, and D. T. Cramb
Department of Chemistry, University of Calgary, Calgary AB, T2N 1N4, Canada

ABSTRACT Two-photon excitation fluorescence cross-correlation spectroscopy (TPE-XCS) is a very suitable method for studying interactions of two distinctly labeled fluorescent molecules. As such, it lends itself nicely to the study of ligand-receptor interactions. By labeling the ligand with one color of fluorescent dye and the receptor with another, it is possible to directly monitor ligand binding rather than inferring binding by monitoring downstream effects. One challenge of the TPE-XCS approach is that of separating the signal due to the receptor from that of the ligand. Using standard organic fluorescent labels there is almost inevitably spectral cross talk between the detection channels, which must be accounted for in TPE-XCS data analysis. However, using quantum dots as labels for both ligand and receptor this limitation can be alleviated, because of the dot's narrower emission spectra. Using solely quantum dots as fluorescent labels is a novel approach to TPE-XCS, which may be generalizable to many pairs of interacting biomolecules after the proof of principle and the assessment of limitations presented here. Moreover, it is essential that relevant pharmacological parameters such as the equilibrium dissociation constant, K_d, can be easily extracted from the XCS data with minimal processing. Herein, we present a modified expression for fractional occupancy based on the auto- and cross-correlation decays obtained from a well-defined ligand-receptor system. Nanocrystalline semiconductor quantum dots functionalized with biotin ($\lambda_{em} = 605$ nm) and streptavidin ($\lambda_{em} = 525$ nm) were used for which an average K_d value of $0.30 \pm 0.04 \times 10^{-9}$ M was obtained (cf. native system $\sim 10^{-15}$). Additionally, the off-rate coefficient (k_{off}) for dissociation of the two quantum dots was determined as 5×10^{-5} s^{-1}. This off-rate is slightly larger than for native biotin-streptavidin (5×10^{-6} s^{-1}); the bulky nature of the quantum dots and restricted motion/orientation of functionalized dots in solution can account for differences in the streptavidin-biotin mediated dot-dot binding compared with those for native streptavidin-biotin.

INTRODUCTION

Biochemical background

Although ligand-receptor interactions have been historically difficult to quantify, recent advances in surface chemistry and fluorescence technology have provided intriguing possibilities for assay development. Recently, it was demonstrated that active receptor proteins can be adsorbed to several surfaces, including glass (1) to make fluorescence-based membrane protein microarrays. Using fluorescently labeled ligands, Fang et al. (1) were able to show binding to specific sites on microarrays. Additionally, they introduced a competition assay based on a nonfluorescent competitor ligand. This is excellent progress toward a heterogeneous ligand-receptor assay, but homogeneous assays (defined as one where the receptor is not bound to the microwell surface) for a specific ligand-receptor have been much slower to develop.

A homogenous assay should be simple, not rely on filtration, and have the capability to deliver binding constants for new ligand entities. Fluorescence-based techniques can be used in this capacity, because fluorescence is inherently highly sensitive and can be selective by labeling ligand and receptor with different colored tags. Association between ligand and receptor could be monitored by fluorescence resonance energy transfer (FRET) or by quenching, but these are inherently high background techniques and suffer from the photochemical instability of organic fluorophores. However, using nanocrystalline semiconductor quantum dots as labels in a two-photon excitation fluorescence cross-correlation spectroscopy (TPE-XCS) assay could mitigate these challenges.

One can envisage a ligand-receptor binding assay where both entities are bound to nanoparticles, leading to the association of the nanoparticles. The desirable stronger interaction of a new ligand with the receptor would be monitored by following the dissociation of nanoparticles. One would need to characterize the parameters of the ligand-receptor interactions and assess the influence of the nanoparticles on binding. Once ligand-receptor binding between nanoparticles has been confirmed and quantified, the new ligand entities can be assessed by their ability to competitively knock the standard ligand-nanoparticles off the receptor nanoparticles. If the two nanoparticles emit light at different peak wavelengths, then a successful test ligand would reduce the amount of associated nanoparticles with two-color emission.

TPE-XCS can provide a zero-background approach to directly measure ligand receptor binding rather than monitoring the downstream effects of binding. In XCS, fluorescence intensities from two spectrally separate fluorophores are

Submitted June 28, 2005, and accepted for publication October 27, 2005.

Address reprint requests to Dr. David T. Cramb, Dept. of Chemistry, University of Calgary, 2500 University Dr. NW, Calgary AB, T2N 1N4, Canada. Tel.: 403-220-8138; Fax: 403-289-9488; E-mail: dcramb@ucalgary.ca.

0006-3495/06/02/1396/15 $2.00

doi: 10.1529/biophysj.105.069526

correlated. A cross correlation is only generated when the two detection channels measure synchronous fluorescence fluctuations. This suggests that the red and green labeled species must be physically linked. Importantly, it is possible to work at low concentrations with reasonable accuracy (2). Fluorescence contribution from individually labeled fluorophores in solution time averages to zero, making XCS a zero background technique (3). Any change in the cross-correlation signal is directly related to the ligand-receptor equilibrium mixture, thus binding information can be directly extracted from the fluorescence correlation and cross-correlation data output. Two-photon excitation has the advantage over one-photon XCS of facilitating simultaneous excitation of two or more different fluorophores with a single laser, reduces out of focus photodamage, eliminates the need for aligning two different colored excitation laser beams, and removes the need for pinholes on the detector side of the optical path.

There are a growing number of examples of correlation spectroscopy used in the examination of ligand binding. These studies have largely examined binding indirectly through quantifying the loss of free fluorescently labeled ligand in the presence of the receptor, both in solution and in living cells. Examples of receptors recently examined include 5-hydroxytryptamine type 3As receptor (4) A1-adenosine receptor (5–6) and endothelin A receptor (7). Also, in many of these studies ligand binding to a cell receptor protein has been inferred through a drastic change in the ligand's diffusion behavior (5–7). In fact, it is only possible to discern the binding of a fluorescently labeled ligand through changes in the diffusion coefficient if the relative molecular weight of the bound ligand is 4–8 times greater than the free ligand (7). Therefore, it is in principle more facile to use the correlation amplitudes ($G(0)$'s and $G_X(0)$'s) derived from FCS and fluorescence cross-correlation spectroscopy (XCS) because they are related to the concentrations of the labeled species and can be used to determine the concentration of bound species directly (2). Although XCS has been applied to protein-protein (2), DNA-DNA (8–9), and lipid-DNA (10) interactions and vesicle fusion (11), XCS has been used to measure ligand-receptor interactions (12) only once, likely because of the challenges in fluorescently labeling receptor proteins. Traditionally, receptor proteins are labeled either using fluorescent protein constructs or via labeled antibodies. Fluorescent proteins are challenging to work with in XCS because most have a long red tail to their emission spectra, which leads to significant cross talk in an XCS application. Detection filters can be chosen to help eliminate this, but only at the sacrifice of sensitivity, because a significant fraction of the emitted photons would be rejected by the detection filter. Furthermore, the expression and purification of fluorescent protein constructs is far from trivial. Hwang and Wohland (12) used organic dye labeled streptavidin and biotin to show the proof of principle for one-color single-photon excitation XCS for ligand-receptor binding. In their communication, Hwang and Wohland (12) also presented evidence for binding between biotinylated fluorescein and a streptavidin functionalized quantum dot (655 nm).

Luminescent semiconductor nanocrystals, or quantum dots (QDs) have many potential advantages in the development of TPE-XCS-based ligand-receptor binding assays. QDs are now used as fluorescent labels for multicolor imaging in biological samples (13). The major advantages of QDs for imaging are: broad excitation spectra, narrow Gaussian emission spectra, low photobleaching yield, and large brightness. Additionally, QDs have several features motivating their use as fluorescence labels for multiphoton imaging in biological systems. Firstly, the particles themselves have significant two-photon absorption cross sections, much larger than existing organic labels (14). Secondly, QDs can be functionalized with a variety of biomolecules making them compatible with a variety of environments and bio-functionalized for nanosensor and fluorescence tagging applications (15–23). Water soluble QDs functionalized with biotin or streptavidin are commercially available in a number of emission wavelengths.

There are many potential advantages of a quantum dot system for TPE-XCS. The first is the spectral characteristics and brightness of quantum dot as labels allow interrogation of ligand-receptor interactions at very low ligand concentrations (approaching 0.1 nM). This physiologically relevant concentration regime is not accessible using standard assays. The narrow emission spectra of quantum dots provide complete separation of signals for the ligand and receptor. Thus, TPE-XCS becomes a truly background-free technique using quantum dots. Also, it is important to determine the limitations of quantum dots in binding assays. It is critical to determine the degree to which the bulky quantum dots affect the binding constants and kinetics of the system they label. Therefore, in a study such as the current one, insight is gained into the effect on the biomolecules because of conjugation to the dot. Finally, the high sensitivity of the quantum dot XCS approach could provide insight into the ligand-receptor system itself.

The biotin-streptavidin system is a natural choice to study ligand-receptor interactions using quantum dots, because it is often used as a model for ligand-receptor binding (24,25). In fact, this system represents a very tight binding interaction with a high K_d (10^{-15}) and a very slow off-rate for biotin (k_{off} $\sim 5 \times 10^{-6}$ s^{-1}) (24). Tetrameric streptavidin is composed of four β-barrels and biotin fits into the end of each barrel in a binding pocket. Thus, the binding ratio for free streptavidin-biotin is 1:4. The main feature responsible for tight binding is a surface loop, which then essentially closes ensuring that the dissociation of biotin would come at a huge energetic cost (24,25).

In this work, we describe a ligand-receptor binding assay based on quantum dot technology and fluorescence correlation spectroscopy. We have employed quantum dots functionalized with streptavidin (QD_S, $\lambda_{em} = 525$ nm) or

biotin (QD_B, $\lambda_{em} = 605$ nm) to follow the binding equilibrium and kinetics for this model system. We have developed a method of data analysis that is directly related to, and comparable with, conventional pharmacological theory. Moreover, we have used free biotin in a competition assay. We find that conjugation to the quantum dot does affect the binding constant and off-rate for the streptavidin-biotin interaction.

Background theory

At equilibrium it is possible to indirectly characterize the receptor system by measuring the binding of particular ligands. The simplest binding case (i.e., L + R ⇔ LR) is described by the Hill-Langmuir theory and allows for the experimental determination of K_d (dissociation constant). For a ligand (L) and receptor (R) system the equilibrium can be described in Eq. 1 (26):

$$P_A = \frac{C_{LR}}{C_R + C_{LR}} \tag{1a}$$

$$P_A = \frac{C_L}{K_d + C_L}, \tag{1b}$$

where P_A, or fractional occupancy, is defined as the molar ratio of occupied receptor, C_{LR}, to the total receptor concentration, $C_R + C_{LR}$ (Eq. 1a). As will be shown below, P_A can be calculated directly using variables determined from fitting to the cross-correlation and autocorrelation data. By plotting the fractional occupancy versus the concentration of added ligand, C_L, it is possible to determine K_d using Eq. 1b (26). In the literature, this is the most common method of presenting binding data. Equation 1b will be used to examine general trends in the data, but not to determine the value of K_d for the quantum dot system. The assumptions for the model represented by Eq. 1b include a 1:1 binding ratio, and following the completion of the titration, the concentration of the ligand far exceeds the concentration of the receptor. Maximal changes in P_A occur when the concentration of the ligand receptor complex is equal to the concentration of free receptors in the sample. For the quantum dot system used in this study, the first assumption may prove to be invalid.

Because there are multiple receptors and multiple ligands on each quantum dot, one may need to consider a multiple-ligand equilibrium approach to binding. Thus, for n biotinylated quantum dots (QD_B) associating with a streptavidin functionalized quantum dot (QD_S) we have;

$$n\,QD_B + QD_S \Leftrightarrow (QD_B)_n QD_S, \tag{2}$$

where n can be a whole number or a fraction, and possibly <1, if multiple QD_S bind to 1 QD_B. It can be shown that a standard analysis of this equilibrium produces the Hill equation for multiligand binding (27):

$$\ln\left(\frac{P_A}{1 - P_A}\right) = n\ln(C_B) - \ln K_d', \tag{3}$$

where P_A is the fractional occupancy of available binding sites on QD_S, n is the ratio of QD_B/QB_S, C_B is the concentration of biotinylated quantum dots, and K_d' is the dissociation constant for the equilibrium presented in Eq. 2. Additionally, in the absence of cooperativity, taking the nth root of the dissociation constant, K_d', gives the dissociation constant, K_d, for the formation of an individual ligand-receptor complex. In the case where $n = 1$, Eq. 3 is analogous to Eq. 1b.

FCS and XCS data analysis

Fluorescence correlation and cross-correlation spectroscopy is based on the analysis of temporal intensity fluctuations $\partial F(t)$ in fluorescence about the time averages fluorescence intensity, $\langle F \rangle$, from emitters in a well-defined interrogation volume. In the system used presently, the fluorescence signals from QD_S and QD_B are spectrally separable. In general, the normalized fluorescence correlation function is defined by:

$$G_{ij}(\tau) = \frac{\langle \partial F_i(t)\partial F_j(t+\tau)\rangle}{\langle F_i\rangle\langle F_j\rangle}. \tag{4}$$

If we consider two emitting species, QD_S and QD_B, then $G_{ii}(\tau)$ and $G_{jj}(\tau)$ represent the autocorrelation functions for the two species and $G_{ij}(\tau)$ is the cross-correlation function between the signal from the two detection channels (one channel for QD_S and one for QD_B). For bookkeeping, we introduce the specific superscripts, S and B, to represent the correlation functions relative to QD_S and QD_B.

Autocorrelation decays were modeled assuming a Gaussian TPE volume using the following equation (10,11):

$$G_{S(B)}(\tau) = G_{S(B)}(0)\left(1 + \frac{8D_{S(B)}\tau}{r_0^2}\right)^{-1}\left(1 + \frac{8D_{S(B)}\tau}{z_0^2}\right)^{-1/2}, \tag{5}$$

where τ is the lagtime, D is the diffusion constant of the quantum dot, r_0 is the laser beam radius at its focus, and z_0 is the $1/e^2$ radius in the z-direction. The TPE excitation volume ($V = (\pi/2)^{3/2}\ r_0^2 z_0$) was calibrated by measuring the autocorrelation decay for a 100-nM solution of Alexa 488 ($D = 2.8 \times 10^{-10}$ m^2/s) in 50 mM Tris-HCl, pH 8.0. The excitation volume was found to be 3.3 fL ($r_0 = 7.6 \times 10^{-7}$ m and $z_0 = 3.0 \times 10^{-6}$ m). The long working distance objective used in this study makes for a slightly larger excitation volume than with more typical high numerical aperture lenses. In the case of bound dots, the diffusion coefficient in Eq. 5 would represent that of the bound species. Assuming no fluorescence cross talk between the channels (as will be demonstrated in Fig. 2), the $G(0)$ will change according to Eq. 7 below.

Cross-correlation decays were modeled as above using the following equation (10,11):

$$G_X(\tau) = G_X(0)\left(1+\frac{8D_{SB}\tau}{r_0^2}\right)^{-1}\left(1+\frac{8D_{SB}\tau}{z_0^2}\right)^{-½}, \quad (6)$$

where the subscript *SB* represents streptavidin and biotin quantum dots that are physically bound together and thus dual-color labeled. Nonlinear least squares fitting to the data was accomplished using the software package, Origin. The equations contain no terms to account for quantum dot blinking, the effects of which were minimized here by keeping the excitation rates low. Also, we observed no fluorescence resonance energy transfer or fluorescence quenching in the case of bound quantum dot systems.

It will be demonstrated that it is possible, simply using $G(0)$'s, to calculate the fractional occupancy, P_A. In the absence of cross talk between the two detection channels, the correlation and cross-correlation amplitudes are given by (8):

$$G_{S(B)}(0) = \frac{\langle C_{S(B)}\rangle + \langle C_{SB}\rangle}{N_A V_{eff}(\langle C_{S(B)}\rangle + \langle C_{SB}\rangle)^2}, \quad (7)$$

and

$$G_{SB}(0) = \frac{\langle C_{SB}\rangle}{N_A V_{eff}(\langle C_S\rangle + \langle C_{SB}\rangle)(\langle C_B\rangle + \langle C_{SB}\rangle)}, \quad (8)$$

where, N_A is Avogadro's number, V_{eff} is the effective TPE volume, $\langle C_{SB}\rangle$ represents the time-averaged concentration of dually labeled specie, and $\langle C_{S(B)}\rangle$ represents the time-averaged concentration of streptavidin (or biotin) functionalized quantum dots. Recall that fractional occupancy is described as the fraction of occupied receptors ($\langle C_{SB}\rangle$) over the total number of receptors in the sample ($\langle C_{SB}\rangle + \langle C_S\rangle$). The expression that describes this relation in terms of concentrations of dually labeled, or occupied receptors and unoccupied receptors are given by Eq. 9:

$$P_A = \frac{\langle C_{SB}\rangle}{\langle C_S\rangle + \langle C_{SB}\rangle}. \quad (9)$$

This relation can be expressed in terms of $G(0)$ values as shown in Eq. 10 and the resulting expression for fractional occupancy is given by Eq. 11:

$$\frac{\langle C_{SB}\rangle}{\langle C_S\rangle + \langle C_{SB}\rangle} = \frac{G_{SB}(0)\cdot N_A V_{eff} G_S(0)}{N_A V_{eff} G_S(0)\cdot G_B(0)}, \quad (10)$$

therefore,

$$P_A = \frac{\langle C_{SB}\rangle}{\langle C_S\rangle + \langle C_{SB}\rangle} = \frac{G_{SB}(0)}{G_B(0)}. \quad (11)$$

MATERIALS AND METHODS

Biotinylated and streptavidin conjugated quantum dots (QDot 605 and QDot 525, respectively) were purchased from Quantum Dot (Hayward, CA) and used as delivered. Stock solutions were stored at 6°C and diluted to desired concentrations using a borate buffer pH 8.3. Before dilution the stock was gently vortexed for 5 min to uniformly disperse the QDots. The diluted solutions of biotin (20 nM) and streptavidin (~1–2 nM) quantum dots were again vortexed to obtain maximum dispersion. To characterize fully the titration curve intermediate stock solutions of 10 and 5 nM QD_B were also prepared. For the titration experiments, 250 μL of the streptavidin solution was placed in a homebuilt quartz sample chamber and placed on a Zeiss Axiovert 200 (Mississauga, ON) microscope. A series of autocorrelation decays were collected for 30, 60, 120, and 300 s. This was done to verify adequate dispersion and limited aggregation of quantum dots in the sample. A cross-correlation scan was collected in the absence of biotin to ensure no green emission from the streptavidin was being detected in the red channel. Once the streptavidin sample had been fully characterized, biotinylated quantum dots were titrated into the sample in aliquots of 0.5–3 μL at a time, until 25 μL of the 5–20 nM biotinylated QDots solution had been added. Following each addition, the sample was agitated and left to equilibrate for 5 min before binding data were collected. Immediately following the equilibration period, red and green autocorrelation decays were collected followed by cross-correlation decays. Importantly, the total volume of biotin added did not exceed 10% of the total volume to ensure that the concentration of streptavidin (receptors) does not change substantially because of dilution.

Competition assays used unlabeled 99% pure d-biotin (Sigma Aldrich, Oakville, ON). A stock solution of 1.61×10^{-3} M in pure water and stored at 6°C was used. A further dilution to 1.61×10^{-7} M was made immediately before each titration. Solutions were vortexed on a low to medium setting to achieve maximum dispersion of d-biotin before sampling.

Samples were excited using 780-nm, 100-fs laser light from a Spectra Physics (Palo Alto, CA) Tsunami laser operating at 82 MHz. The laser power was attenuated to 20 mW with a neutral density filter to avoid photodamage. QDot 525 and QDot 605 both have appreciable two-photon excitation probability at 780 nm. The laser beam was expanded using a Galilean telescope to slightly overfill the back aperture of a 40×, 0.9 N.A. Zeiss objective lens (working distance = 2 mm) mounted on a Zeiss Axiovert 200 fluorescence microscope. TPE-fluorescence was collected by the same objective lens, passed through a broad bandpass filter to remove laser light (Omega Optical, XF3100, Brattleboro, VT) and reflected off a dichroic optic (Chroma, 700DCSPXR, Rockingham, VT) and through a tube lens in the side port of the microscope. A second dichroic optic (Chroma 565DCLP) is used to separate the red and green fluorescence. The spectrally separated light passes through bandpass filters (Chroma, E590LPv2 and D535/50× for the red and green emission, respectively) and is coupled into optical fibers located at the focus of the tube lens. Using the optical fibers, the fluorescence is detected by two Si avalanche photodiodes (APDs, Perkin-Elmer, SPCQ-200, Fremont, CA). The output of the APDs was analyzed using a correlator card (ALV-5000, Langen, Germany).

RESULTS

To understand and quantify the binding between quantum dots functionalized with streptavidin (QD_S) and biotinylated quantum dots (QD_B), a titration of QD_S with QD_B was performed as described in the Materials and Methods section. Using TPE-FCS and TPE-XCS $G(0)$ values and diffusion coefficients for red, green, and dually labeled species were determined. The $G(0)$ values could then be used (Eq. 11) to calculate the fractional occupancy for each titration point.

FCS of quantum dots

Control experiments that examine the behavior of $G_B(0)$ and $G_S(0)$ under the titration conditions, were carried out. A typical series of autocorrelation decays for a range of QD_B concentrations are given in Fig. 1. The solutions represented in this figure were created by adding small aliquots (1–3 μL) of stock QD_B solution (20 nM) into 250 μL of buffer. The

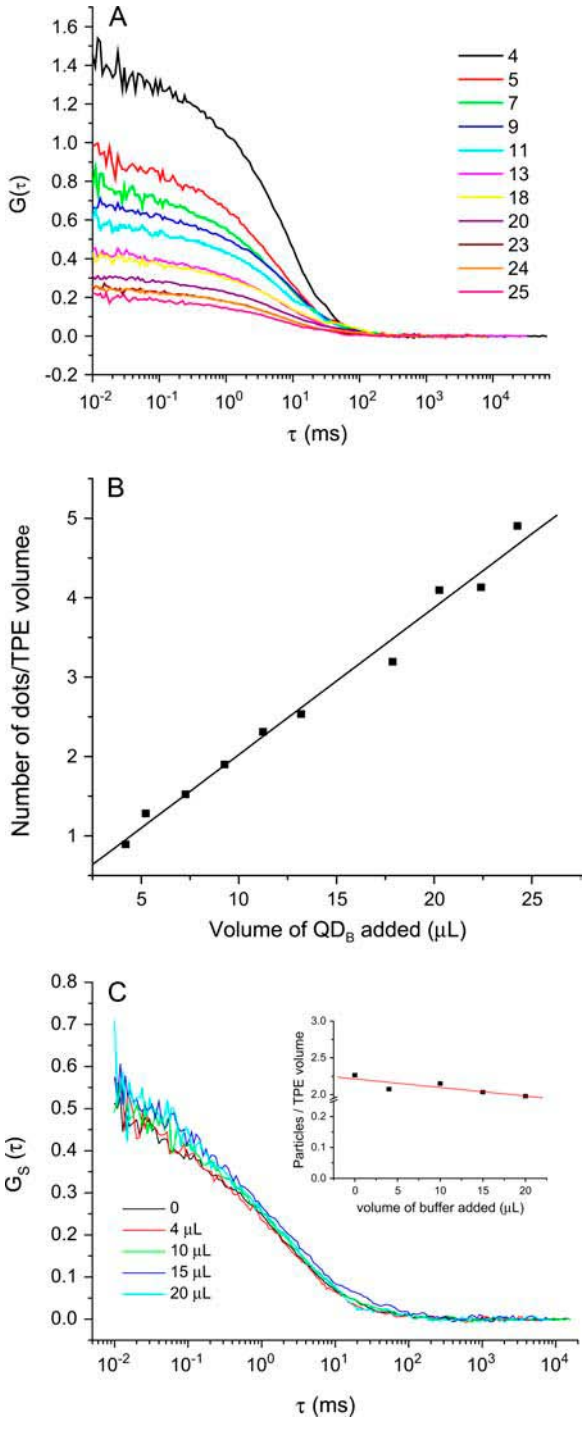

FIGURE 1 (*A*) Autocorrelation decays for QD_B in borate buffer. Note that as the volume of QD_B added to the solution increases, the $G(0)$ become smaller. The inset depicts the volumes of QD_B added in microliter units. (*B*) To further illustrate the relationship between the measured $G(0)$ values the average number of particles in the excitation volume, $(G(0)^{-1})$, was plotted against the volume of QD_B added. From Eq. 6, $G(0)$ should be inversely proportional to the average number of particles in the excitation volume. (*C*) Autocorrelation decays for 1 nM QDS as a function of borate buffer volume added as a mock titration. The inset depicts the volumes of QD_B added in microliter units. The inset is a plot of the average number of QD_S particles in the excitation volume, $(G(0)^{-1})$ was plotted against the volume of buffer added.

autocorrelation decays were fitted using Eq. 5 from which $G_B(0)$ and D_{QDB} were obtained. This allowed us to verify that the change in total solution volume over the titration was insignificant and therefore that the concentration increase for added QD_B was linear (Fig. 1 *B*) and that the concentration of QD_S was essentially constant. This is depicted in Fig. 1 *C*, where there is minimal change in the autocorrelation decay of QD_S as a function of buffer added, over the same volume range used in the titrations. The total change in volume upon completion of the titration was $<10\%$, thus maintaining an approximately constant receptor concentration.

From the fit to the QD_B autocorrelation decays, the average diffusion coefficient for the biotinylated QDots was found to be 1.7×10^{-11} m^2/s, and the average hydrodynamic radius of the dots was determined as 14 ± 3 nm using the Stokes-Einstein relation. The temperature for the calculation was 20°C and the viscosity of the buffer was estimated to be the same as that of water. The buffer employed had low salt and BSA content and thus a viscosity very close to that of pure water. Similar fits to the QD_S autocorrelation decays (data not shown) produced an average diffusion coefficient for streptavidin functionalized dots in solution of 3.6×10^{-11} m^2/s. This value correlates to an average hydrodynamic radius of 8 ± 3 nm. The quantum dots are close in size within measurement error, with the red dots being slightly larger. One should recall that the hydrodynamic radius represents the core, shell, and polymer coating containing the biofunctional group (28).

One of the major advantages of using quantum dots for cross-correlation studies is that their narrower emission spectra minimize the cross talk between detection channels. In Fig. 2 autocorrelation decays and count rate trajectory plots are presented. Each panel depicts a solution containing a single type of quantum dot. Fig. 2 *A* represents the data that was collected from a 1.5-nM solution of QD_S (*green*). The green decay (*squares*) is typical for green quantum dots and the red decay (*circles*), which would represent cross talk, is only noise. From the inset in Fig. 2 *A* it is notable that the mean count rate is 8.5 kHz in the green channel and 0.35 kHz in the red channel. The 0.35-kHz signal is solely due to dark counts (~0.2 kHz) and laser scatter (~0.15 kHz). Fig. 2 *B* represents a solution of 3.0 nM QD_B (*red*). Here a typical autocorrelation decay of the red quantum dots is found in the red plot (*squares*), whereas the green plot (*circles*) for the green dots is again only noise. The inset of panel *B* shows that there are mean count rates of 11.1 and 0.3 kHz in the red and green channels, respectively. Here, the signal in the green channel is also solely due to dark counts and laser scatter. Thus, for both solutions, no measurable autocorrelation decay was generated by cross talk between channels, indicating that the signals were completely spectrally separated (29).

Titrations of QD_S with QD_B

Titrations of QD_B into ~1 nM solutions of QD_S were carried out in triplicate. Cross-correlation and autocorrelation decays

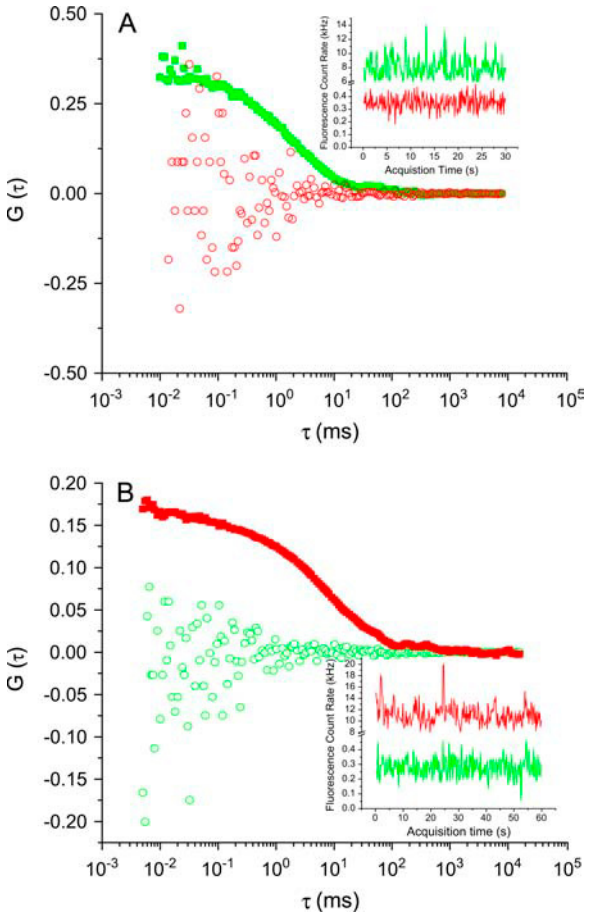

FIGURE 2 Autocorrelation decays for: (*A*) QD_S ($\lambda_{em} = 525$ nm) and (*B*) QD_B ($\lambda_{em} = 065$ nm). (*A*) The green squares represent the green channel decay for a solution of 1.5 nM QD_S and the red decay (*circles*) is the signal from the red autocorrelation channel, collected simultaneously. In the inset, the green line represents the green channel count rate (mean count rate = 8.5 kHz). The red line represents the count rate trajectory from the red detection channel (mean count rate = 0.35 kHz) for this solution. (*B*) The red squares represent the red channel decay for a solution of 3.0 nM QD_B and the green decay (*circles*) is the signal from the green autocorrelation channel, collected simultaneously. In the inset, the red line represents the red channel count rate (mean count rate = 11.1 kHz). The green line is the green channel count rate (mean count rate = 0.3 kHz) for the same solution. These decays and trajectories illustrate that there is no cross talk between the detection channels.

were recorded for each equilibrated point in the titration. Fig. 3 *A* represented a series of cross-correlation decays observed as a function of increasing biotinylated quantum dot concentration. Fig. 3 *B* depicts a typical fluorescence count rate trajectory for a solution containing both QD_S and QD_B. From the lack of the change in the average fluorescence count rate in the QD_S trajectories as a function of QD_B added (data not shown), there was no evidence of fluorescence resonance energy transfer. Also, no evidence of large aggregate formation was observed. Fig. 3 *C* shows a cross-correlation decay and fit using Eq. 6. The correlation decay and fit in Fig. 3 *C* was for the data from the black trace in Fig. 3 *A*. Fig. 3 *D* shows the autocorrelation decays of QD_S as a function of QD_B added. The increase in $G_S(0)$ suggests that the number of QD_S particles is decreasing with QD_B added, consistent with a binding QD_S/QD_B ratio >1. The derived diffusion coefficients from fitting these QD_S autocorrelation plots using Eq. 5 are given in the inset of Fig. 3 *D*. A trend of decreasing D is consistent with binding taking place. Unfortunately, it was not possible to perform a global analysis using sums of the diffusion coefficients similar to the approach of Eggeling et al. (30). The signal/noise was insufficient to allow a unique decomposition of the diffusional part of the correlation decays into 1:1 and 2:1 QD_S/QD_B components.

Control experiments were carried out to insure that there was minimum nonspecific binding. Nonbiotinylated red quantum dots were added to streptavidin dots. Fig. 4, *A* and *B*, represent the fluorescence trajectory and the cross correlation, respectively, when 1.1 nM unlabeled quantum dots were added to the 1.0 nM streptavidin sample. Note that although there were intensity spikes present in both channels (4A), no appreciable cross correlation (i.e., $G_X(0) < 0.02$) was found for the control. Using biotinylated red dots under the same conditions gave a cross-correlation amplitude ($G_X(0)$) of 0.30 (Fig. 4 *C*).

Binding plots of QD_S-QD_B interactions

As one follows the behavior of $G_X(0)$ versus the volume of QD_B solution added (Fig. 5), there appears to be at least three regimes. The first is where $G_X(0)$ increases with increasing QD_B. The second where there is a precipitous drop in the $G_X(0)$ and finally leveling off of the plot. It is difficult to extract relevant binding data from this plot, because the $G_X(0)$'s contain information on all species in solution. However, a plot of P_A as derived from $G_X(0)$ and $G_B(0)$ is more illuminating.

Fig. 6 represents a cumulative concentration-occupancy plot for QD_S and QD_B. This plot contains the data from three different titrations series and the data are presented in a format consistent with Eq. 1b. Table 1 summarizes the constants obtained from the series of three concentration occupancy plots. The average K_d (determined by fitting Eq. 3 to the data) does not change substantially (within mean ± 3 SD) with change in streptavidin concentration. Additionally, the average radius of the cross-correlated species remains constant within the margins of error for each of the three titrations. Interestingly, these occupancy plots never approach $P_A = 1$, which suggests that a single site binding model may not be appropriate for QD_S-QD_B interactions. According to the manufacturer, each QD_S and QD_B supports more than one streptavidin and more than one biotin, respectively. Given the size of the quantum dots, it is possible and even likely that the dots bind in 2:1 ratios. If this is the case, Eq. 1b no longer adequately represents the binding data. Analysis of the binding data using Eq. 3 (the

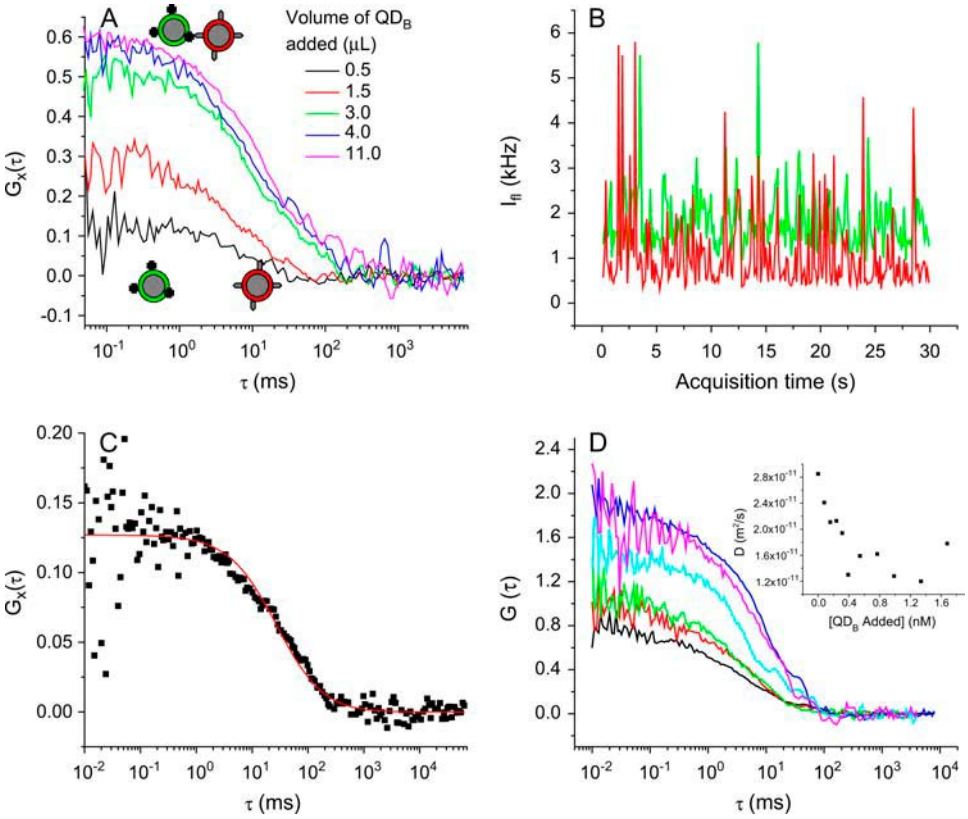

FIGURE 3 (*A*) Cross-correlation decays observed for a single QD_S population with increasing QD_B added. For these titration conditions, $G_x(0)$ increases as a function of QD_B added and then inflects at a value of ~0.6. (*B*) Fluorescence count rate trajectory for a typical titration data set. In this case, there was a total of 1 nM QD_S and 0.1 nM QD_B in the solution. (*C*) The data (■) and result of a fit to the data using Eq. 5 (*line*). (*D*) Autocorrelation decays of QD_S as a function of QD_B added. The $G(0)$ values increase, suggesting a lowering of the QDS concentration. This is consistent with a fraction of the bound QD_S:QD_B particles having a 2:1 ratio. The inset plots the fitted diffusion coefficient of QD_S as a function of QD_B added. The diffusion coefficient becomes smaller and then levels off consistent with binding and lack of high order aggregates. See text for discussion.

Hill equation) should provide insight into the possibility of multiple dot interactions.

Fig. 7 shows a plot of the binding data using the Hill equation (Eq. 3). From this plot, we obtain a K_d of 0.30 ± 0.04 nM and a binding ratio of $QD_S/QD_B = 1.5$. The binding ratio suggests that there is likely a heterogeneous mixture of 1:1 and 2:1 (QD_S/QD_B) at equilibrium. As will be elaborated in the Discussion, direct comparison with streptavidin-biotin binding ratios is not warranted, because the dots themselves are so much larger than the ligand and receptor. The Hill equation is developed assuming that there is no cooperativity in the multiple binding and the analysis reflects this, because there is no evidence of multiple slopes in the plot.

Competition assay using free d-biotin

Competition assays for the QD_S-QD_B system can serve multiple purposes. First, by using free biotin to compete with QD_B for QD_S binding sites, a deeper understanding about the nature of the streptavidin on the quantum dot surface will be gained. Second, it may be possible to elucidate the number of available streptavidin sites on the QD surface. Finally, using competition assays one can measure the off-rate for unbinding.

Free biotin was used to displace the QD_B ligand from QD_S. In separate experiments, two different concentrations (61 and 119 μM) of d-biotin were added to mixtures of QD_S/QD_B; 1.0:0.7 nM, respectively. P_A was measured at shortly after (5–15 min) addition of the d-biotin and then at 4, 24, and 48 h after addition. The data are presented in Fig. 8 *A* and represent the lowering of P_A as the dissociation proceeds.

If we consider the simplifying scenario of a 1:1 pair, QD_S:QD_B, in equilibrium with the free quantum dots, QD_S and QD_B, we can write the following equilibrium equation:

$$QD_S : QD_B \underset{k_{on}}{\overset{k_{off}}{\leftrightarrow}} QD_S + QD_B. \tag{12}$$

Adding free d-biotin to this system can be approximated as a perturbation that removes free QD_S, thus promoting more dissociation of QD_S:QD_B to restore equilibrium. The following integrated rate equation was used to fit the data:

$$\frac{P_A(t)}{(P_A)_0} = \frac{1}{1 + \Delta P_A}\left[\Delta P_A + e^{-k_{off}(1 + \Delta P_A)t}\right]. \tag{13}$$

It has only one adjustable parameter, k_{off}, which represents the rate constant of QD_S:QD_B unbinding. ΔP_A is related to the initial and final P_A for this competition. The derivation of this equation can be found in the Appendix.

It was also possible to begin with QD_S-d-biotin and compete off the d-biotin with QD_B. In this assay, it should be possible to observe the increase in P_A. The reverse competition assay was performed where free biotin was equilibrated with QD_S and then QD_B was added into that solution. Details of this displacement reaction are given as follows: unlabeled biotin (10.0 nM) was added to two QD_S samples

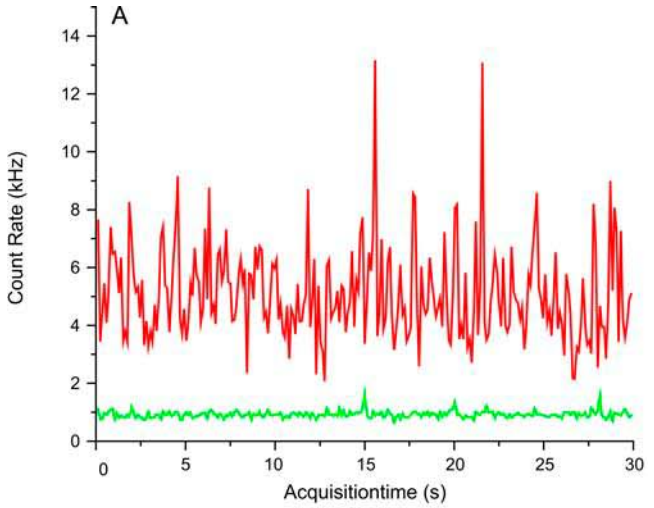

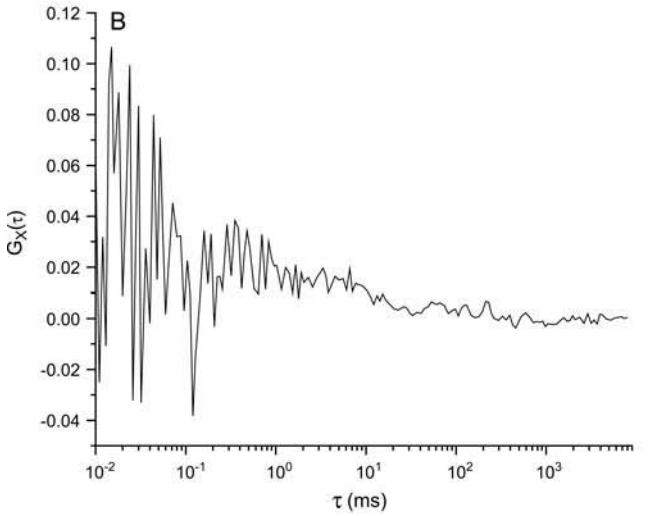

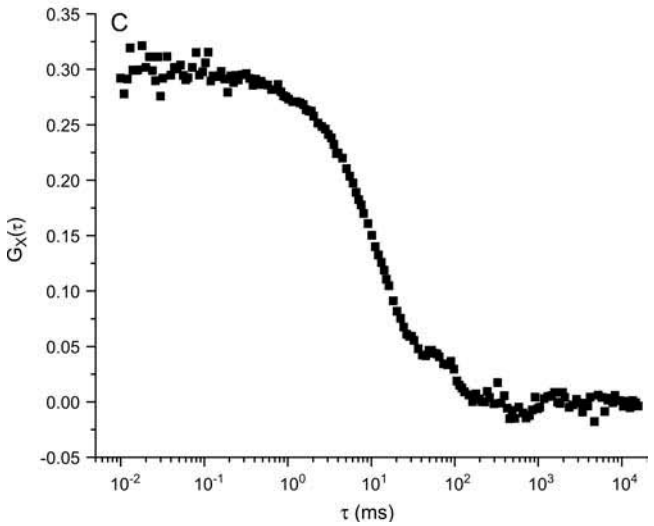

FIGURE 4 Quantum dot nonspecific binding control experiments. (*A*) The count rate trajectory for the mixed sample containing nonfunctionalized QD605 (*red*) and QD_S (*green*). (*B*) The resulting cross-correlation decay in which no significant cross correlation is detected. The solution contained 1 nM each of QD605 (*red*) and QD_S (*green*). (*C*) For comparison, the equivalent solution to the control experiment, but using QD_B.

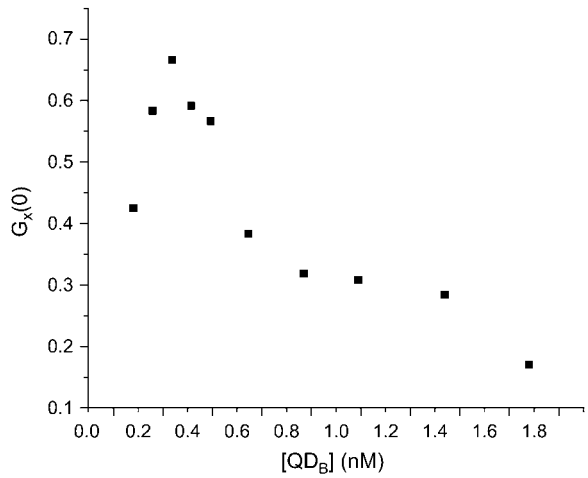

FIGURE 5 A plot of the $G_x(0)$ values obtained for several additions of QD_B to a 1-nM solution of QD_S. The plot suggests at least three regimes in the binding curve. The first region in which $G_x(0)$ increases with increasing QD_B occurs at low concentration. Then a drop in the measured $G_x(0)$ value is observed. Finally, the measured $G_x(0)$ value displays a monotonic decrease.

(of the same concentration 1.0 nM). Following equilibration of the QD_S-biotin system, QD_B was added to the mixtures to give concentrations of 1.4 and 2.08 nM. P_A was measured for the two samples at 5 min, 4, 24, 48, 72 and 96 h postaddition of QD_B. Fig. 8 *B* illustrates the kinetic growth of P_A versus time for both samples.

The kinetics representing an increase in P_A observed for the dissociation of QD_S:dB are more complex. Here, we have to consider two reactions:

$$QD_S : dB \underset{k'_{on}}{\overset{k'_{off}}{\leftrightarrow}} QD_S + dB, \tag{14}$$

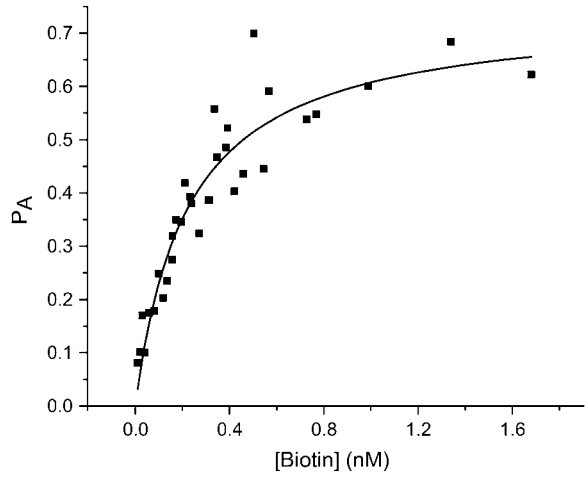

FIGURE 6 A concentration-occupancy plot. The value for the fractional occupancy, P_A, was calculated using Eq. 9. Note that this concentration-occupancy plot has the same shape as conventional Hill-Langmuir concentration occupancy plots. The K_d derived from Eq. 1b has the value 0.22×10^{-9}.

TABLE 1 Summary of streptavidin-biotin QDot titrations

Titration	Streptavidin concentration (nM)	Average diffusion coefficient of dually labeled species (m^2/s)	Average radius* of dual labeled species (nm)	K_d from fitted data (nM)
1	0.54 ± 0.09	7.29×10^{-12}	34 ± 5	0.24 ± 0.05
2	1.38 ± 0.04	9.02×10^{-12}	28 ± 4	0.32 ± 0.08
3	0.75 ± 0.02	7.60×10^{-12}	33 ± 5	0.25 ± 0.10
Cumulative				0.22 ± 0.04

*Radii are calculated by entering the diffusion coefficients presented in this table into the Stokes-Einstein relation, $r = kT/(6\pi\eta D)$, where k is the Boltzmann constant, T is temperature (293 K), and η is the solution viscosity (0.001 Ns/m^2).

$$QD_S + QD_B \underset{k_{off}}{\overset{k_{on}}{\leftrightarrow}} QD_S{:}QD_B. \tag{15}$$

If we assume the free QD_S is rapidly consumed by the free QD_B, then the reverse reaction in Eq. 15 can be neglected. Therefore, the forward reaction of 14 is the rate-limiting step. We can then write the following rate law:

$$P_A(t) = \frac{k'}{k' + k_{off}}\left[1 - \left(1 - \frac{k'_{off}}{k'}\right)e^{-k'_{off}t}\right], \tag{16}$$

where $k' = k_{on}C_B$. This equation essentially represents an exponential increase in QD_S:QD_B as QD_S:dB dissociates. It has a limitation at long time in that this approach takes into account only 1:1 QD_S:QD_B association. Nevertheless, this approach should be sufficient to obtain an estimate of the QD_S:dB off-rate constant, k'_{off}. The derivation of this equation can also be found in the Appendix.

From the fits in Fig. 8 *A* (QD_S-QD_B dissociation, fit using Eq. 13), it is observed that the competition kinetics do not depend on the competitor concentration. The fits produced the same rate constants within measurement error, 5.2 ± 0.7 × 10^{-5} s^{-1} and 6.2 ± 0.7 × 10^{-5} s^{-1}, respectively, for 119 and 61 μM d-biotin added. The ΔP_A ($\Delta P_A = (P_A)_\infty / [(P_A)_0 - (P_A)_\infty]$) values were 1.2 and 1.5, respectively, for 119 and 61 μM d-biotin added. The larger value could arise from a greater amount of QD_B liberated by the higher concentration of d-biotin added and may also reflect that higher concentrations of d-biotin could dissociate the associated species that were not 1:1.

From Fig. 8 *B* (QD_S-d-biotin dissociation, fit using Eq. 16), one can see that the rate constant for the reaction did not change significantly as a function of labeled biotinylated quantum dot concentration. This indicates that the rate of this reaction is independent of labeled biotin and therefore dependent only on the off-rate of the unlabeled biotin, as expected. From the fit to the model values of 5.2 ± 1.0 × 10^{-5} s^{-1} and 5.8 ± 1.3 × 10^{-5} s^{-1} were recovered for k'_{off},

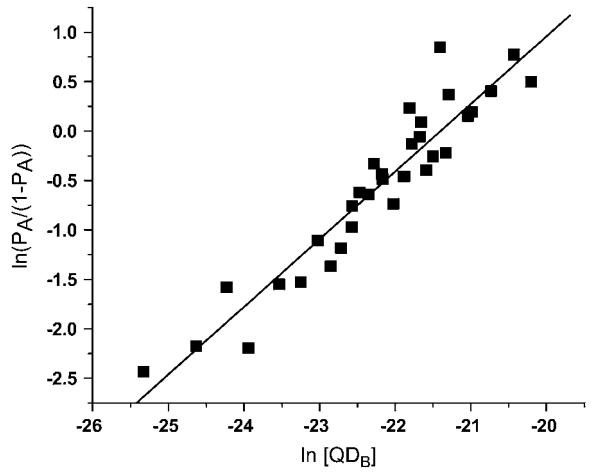

FIGURE 7 A Hill plot of the same data presented in Fig. 6. The Hill plot represents the data linearized to be analyzed using Eq. 3. Thus, the slope of this plot gives the binding ratio and the *y*-intercept allows the determination of K_d, the effective binding constant. From this plot, the ratio (QD_S/QD_B) is 1.5 and K_d is 0.30×10^{-9}.

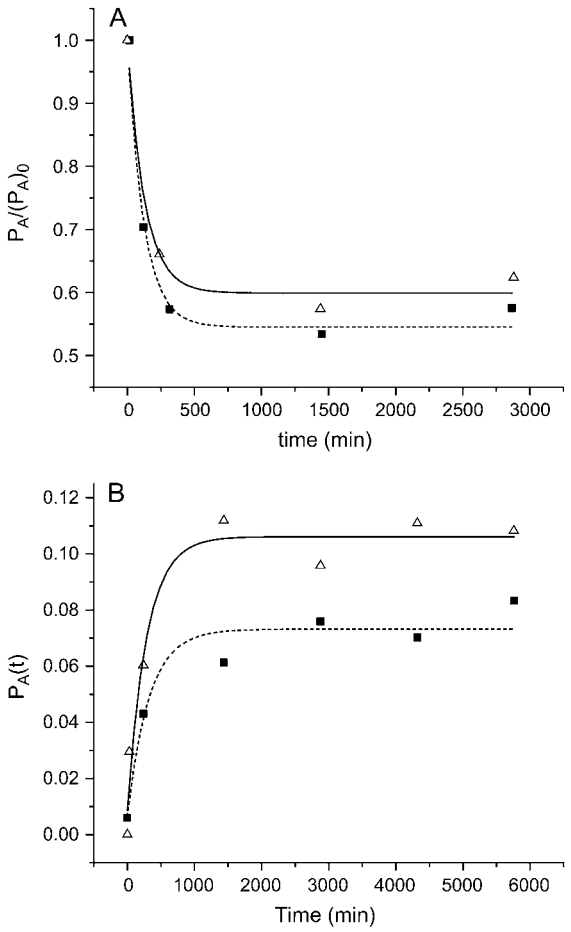

FIGURE 8 Competition assay kinetics. (*A*) Changes in the normalized fractional occupancy, $P_A/(P_A)_0$, versus time for QD_S/QD_B (1:0.7 nM/nM) solution to which 61 μM (■) and 119 μM (△) d-biotin was added. (*B*) Changes in the fractional occupancy, P_A, versus time for QD_S (1 nM) whose streptavidin sites are initially blocked with d-biotin (10 nM). QD_B was added to this solution (1.4 nM (■) and 2.1 nM (△)) and the change in P_A was measured. The dissociation data were modeled using Eq. 12 (*A*) or Eq. 15 (*B*).

for 1.4 and 2.0 nM QD_B added, respectively. The values of the maximum in P_A, as the system approaches equilibrium, reflect the increase in $k'/(k' + k_{off})$, which increases with C_B.

These results suggest that it may be possible to estimate the number of potential sites per QD_S by examining the concentration of free biotin needed to block all the available sites. The kinetics measured above indicates that such a blocking experiment would have to be performed in the first minutes after addition of QD_B to ensure minimal exchange of free biotin with QD_B.

To determine the number of accessible streptavidin sites per dot, a series of 1.0-nM QD_S solutions were prepared and to them varying concentrations of unlabeled d-biotin were added. Following an equilibration time of 10 min for QD_S-d-biotin, 0.23 nM labeled quantum dots, we added to each sample and the mixture was vortexed briefly. Autocorrelation and cross-correlation scans were obtained (within 10 min of addition) to prevent significant exchange of biotin for QD_B. The fractional occupancy for each sample was determined as above using the correlation amplitudes, $G_X(0)$ and $G_B(0)$, and Eq. 11 and plotted versus amount of biotin in the mixture. Fig. 9 represents the average fractional occupancy for each concentration of unlabeled biotin. The graph was constructed by combining the data of three separate experiments.

The linearity of the plot of P_A versus the concentration of biotin in the mixture, suggests that minimal biotin exchange took place during the experiments. Therefore, the plot in Fig. 9 represents the increasing fraction of sites blocked as a function of free biotin loaded into the solution. Thus, the point where the P_A becomes zero represents the concentration of biotin needed for complete blocking of sites streptavidin on the quantum dots. This occurs at ~10 nM of biotin. Because the QD_S concentration was 1.0 nM, there appear to be 10 sites on each QD_S that can be blocked by free biotin. This would mean a maximum of 10 streptavidins per quantum dot, if there was only one active binding site per streptavidin. If all four binding sites remain active, then there are 2–3 streptavidins per dot. Note also, not all 10 sites on QD_S can be occupied by QD_B simultaneously, owing to steric hindrance of the dots.

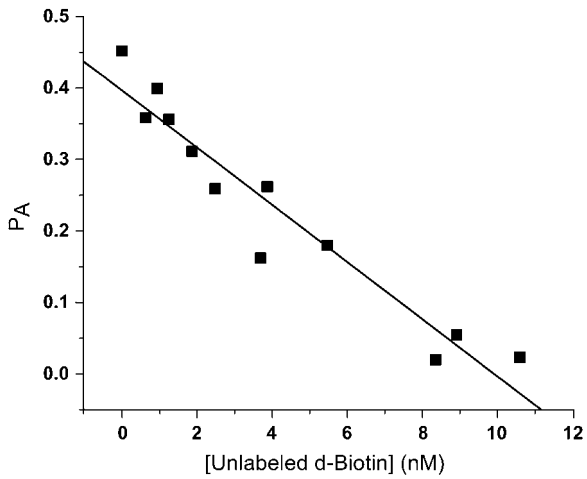

FIGURE 9 Blocking assay to determine the number of biotin binding sites per streptavidin functionalized quantum dot. Binding sites on QD_S (1 nM) were blocked with varying concentrations of d-biotin and the number of remaining free sites was determined using a QD_B binding assay. Thus, the plot of P_A versus concentration of d-biotin has an x-intercept that represents the molarity of d-biotin needed to block all binding sites. This results in a mol ratio of 1:10 QD_S/d-biotin for complete blockage, suggesting that there are on average 10 binding sites per QD_S.

DISCUSSION

Examination of quantum dots using fluorescence correlation spectroscopy

In this article, we describe the development of a ligand-receptor binding assay using two-photon fluorescence cross-correlation spectroscopy of biofunctionalized quantum dots. Quantum dots have several advantages in such assays. Firstly, because of their narrow emission spectra compared with organic fluorescent tags, cross talk between the two detection channels is eliminated, as shown in Fig. 2. Secondly, because most quantum dots have large two-photon excitation cross sections and significant fluorescence quantum yields, their brightness allows single dot experiments to be carried out with relative ease allowing very low concentrations to be measured. Thus, only miniscule amounts of receptors and ligands are needed for such TPE-XCS based assays as described herein. However, there are concerns that the photophysical behavior of quantum dots may obfuscate some XCS results.

The most commonly perceived challenges of using dots in correlation spectroscopy are their propensity to enter a non-emissive state (blinking) and their longer fluorescence lifetimes (10-20 ns) (31,32). The former can lead to anomalies in the interpretation of correlation decays. The latter can lead to saturation of excitation, because the typical laser pulse frequency in TPE-XCS experiments is 80 MHz. Thus, the excited population cannot completely recover before encountering the next laser pulse. Therefore, a careful choice of operating conditions must be made to minimize these effects on the data provided by FCS and XCS.

We have found that reliable concentrations can be determined by operating the Ti:sapphire laser at 20 mW to vastly reduce the effects of blinking. Similar to Webb and co-workers (14) a consistent method of fitting $G(0)$'s to the autocorrelation data was used. We chose the average value of the autocorrelation amplitude ($G(0)$) at a lagtime of 0.01 ms. Also, the linear plots of $1/G(0)$ versus the concentration of QD_B (see Fig. 1 *B*) show that the sample volume does not change significantly under the titration conditions. Because the blinking behavior between dots is not synchronized, no evidence of blinking presented itself in the cross-correlation decays. In addition, fitting the autocorrelation curves to Eq. 5

allowed average diffusion coefficients for QD_S, QD_B, and QD_S:QD_B to be obtained. These diffusion coefficients were used to determine the average hydrodynamic radius for each of the species. Our experiments indicated that the average radius for the streptavidin 525 quantum dot was ~8(3) nm, the biotinylated 605 dot was ~14(5) nm. The numbers in parentheses are means ± 1 SD of the radius in the units given. These values reflect the size of the quantum dot-biomolecule construct and thus have contributions from core, shell, and polymer coating containing the biomolecules. Moreover, these values are calculated presuming that the quantum dot is spherical, which may not be the case for QD_S, because there may not be uniform surface coverage of streptavidin or biotin on the surface. The dually labeled species was ~28–34 (5) nm (determined from the Stokes-Einstein relation; see Table 1). The radius of the dually labeled species suggests that the binding regime for the experimental conditions studied could be a mixture of 1:1 and 2:1 QD_S/QD_B.

Quantum dot binding through streptavidin-biotin interactions

A titration of QD_S with QD_B produced changes in the measured $G_X(0)$ (Fig. 5). Three $G_X(0)$ regimes (increasing, decreasing, and leveling) were observed as a function of added QD_B (Fig. 5). Two of the regimes can be rationalized in terms of Eq. 8. In the mid-titration regime, the concentration bound species (C_{SB}) is comparable with that of the free species (C_S and/or C_B), Eq. 8 becomes inversely proportional to C_{SB}. Finally as the binding sites become saturated, change $G_X(0)$ is dependent (inversely) only on C_B and slowly approaches zero. For the first part of the titration, the increase in C_{SB} is balanced by the increase in total concentration of QD_B. An increasing $G_x(0)$ results from the 2:1 QD_S/QD_B binding ratio that effectively lowers the total concentration of QD_S. This effect is most pronounced at very low QD_B concentrations. These results can be compared qualitatively with those of Hwang and Wohland (12). In their one-photon XCS study, a fluorescein-labeled biotin was found to interact with streptavidin-functionalized red quantum dots. They found trends in $G_X(0)$ as a function of biotin added, similar to those observed in this study and rationalized these qualitatively as different binding regimes for the biotin on the QD_S. Although it is possible to use the $G_X(0)$ versus [QD_B] plot directly, it is illuminating to convert this data into a more traditional concentration/occupancy plot.

We have used the simple binding system of biotin and streptavidin to illustrate the generation of concentration/occupancy plots using FCS and XCS. These plots are analogous to those obtained using conventional binding assays using radioligands and bulk fluorescence. To obtain Hill plots using Eq. 3, it was necessary to derive an expression for P_A (Eq. 11) using the definitions for $G(0)$ and $G_x(0)$ (8). The derived expression for the fractional occupancy of receptor, P_A, results from the fact that $G_X(0)$, contains concentration information for all species, QD_S, QD_B, and QD_S:QD_B. The ratio of $G_x(0)/G_B(0)$ divides out the dependence on biotinylated dots from the cross-correlation-derived concentrations, leaving $\langle C_{SB}\rangle/(\langle C_S\rangle + \langle C_{SB}\rangle)$, which is equal to P_A.

Using Eq. 3, P_A vs. [QD_B] data were plotted to extract relevant binding parameters (ratio of QD_S/QD_B and K_d) for the QD_S-QD_B binding systems. The derived K_d for the system under investigation was 0.3 ± 0.04 nM. The equilibrium binding ratio was 1.5 (QD_S/QD_B), indicating a mixture of 1:1 and 2:1 species, which is reflected in the diffusion coefficients mentioned above. The K_d value is substantially larger than the native value (~10^{-15} M). Experiments carried out by Huang et al. (33) using streptavidin-coated polystyrene spheres obtained similar reduced binding interactions due to the bulky nature of the solid support. The K_d values reported by Huang et al. (33) are between 0.09–20 nM, with larger K_d values resulting from the streptavidin and biotin being linked to increasingly larger polystyrene and DNA supports. It was concluded from this study that the association of the bulky DNA to the biotin reduced the mass transfer to the surface of the streptavidin polystyrene coated spheres. Additionally, they report exponentially reduced binding constants for increased ligand bulk, thus validating the reduced binding observed in the current study. The streptavidin coated polystyrene spheres used in the work by Huang et al. (33) study were an order of magnitude larger than the quantum dots used in the current study, but the biotinylated DNA ligands were on the same order of size as the biotinylated quantum dots.

Effect of quantum dots on ligand-receptor interactions

It is important to understand the effect of the quantum dots on the ligand-receptor binding system being studied. This will provide information on the potential advantages and limitations of QD-based assays. With this in mind, we set out to establish the number of streptavidin binding sites per quantum dot and use that information to examine whether changes in the k_{on} and/or k_{off} could account for the difference in K_d for the quantum dot system compared with that for free streptavidin-biotin binding.

By blocking the available binding sites on the QD_S with d-biotin, we were able to determine the number of binding sites per QD_S available to QD_B. Because each tetrameric streptavidin would act as a maximum of four independent sites (24), we expected that by adding 5–10 equivalents of unlabeled d-biotin (based on an estimate of surface area of the dot) essentially no QD_S-QD_B binding would be measured. Examination of Table S1 (Supplementary Material) and Fig. 9 illustrate that at 10.6 nM of unlabeled d-biotin (~10 equivalents) the fractional occupancy was reduced to almost zero. Thus, there are 10 biotin binding sites per QD_S. From Table S1 we also note that the average hydrodynamic radius of the dually labeled species decreases with increased blocking. Under the conditions of these experiments, when

no d-biotin is present we note a 2:1 binding regime of QD_S/QD_B based on the fitted diffusion coefficients. At 10.6 nM d-biotin, the few remaining dually labeled species are present in a 1:1 binding regime. As expected, the binding of d-biotin lowers the number of available sites such that the most likely complex is 1:1.

It is possible that the off-rate for QD-biotin from the quantum dot-bound streptavidin contains information about how the QD perturbs both the biotin binding site and the biotin ligand. If the reduced binding coefficient is a result of changes in the binding pocket or capping peptides (24), this should manifest in a faster off-rate for the QD_B- and d-biotin-QD_S than for native biotin-streptavidin. Competition assays were used to obtain the off-rate coefficient for the QD_B-QD_S and for the unlabeled d-biotin-QD_S interactions. Fig. 8 indicates that the reaction rate does not change as a function of competitor concentration. Thus, the results are consistent with the dissociation of QD_B-QD_S or of QD_S-d-biotin being the rate-limiting step. The rate constant for both QD_B-QD_S and QD_S-d-biotin dissociation are approximately the same ($k_{off} \sim 5\text{-}6 \times 10^{-5}\ s^{-1}$; Fig. 8 *A*) and have values 10× faster than the off-rate ($k_{off} \sim 5 \times 10^{-6}\ s^{-1}$) (24) characteristic for the native biotin-streptavidin system. The larger off-rate constant for this study could result from inhibition of streptavidin loop closure due to the bulk of the quantum dot.

The difference in off-rate constants does not account for the difference in K_d between the dot system (3×10^{-10}) and the native system (10^{-15}), which suggests that the changes in binding also result from a lower value for the on-rate coefficient ($k_{on} = k_{off}/K_d$) for the quantum dot system. A smaller value for k_{on} could result from a combination of the slower diffusion coefficient for the dot system and slower orientation dynamics due to the bulk of the dot system. We can make a simple estimate of the differences in k_{on} assuming that only the frequency factor, A_{free} vs. A_{QD}, changes in the Arrhenius expression for the rate coefficient. Here the subscript, ''free'', represents the kinetics of freely diffusing native streptavidin and biotin, and ''QD'' represents streptavidin and biotin bound to quantum dots. To examine this hypothesis qualitatively, we can use the ratio:

$$\frac{k_{on_{free}}}{k_{on_{QD}}} = \frac{A_{free}}{A_{QD}} = \frac{frac-avail_{free} * ((r_{SB})(1/r_S + 1/r_B))_{free}}{frac-avail_{QD} * ((r_{SB})(1/r_S + 1/r_B))_{QD}}, \tag{17}$$

where r_{SB} is the encounter distance for binding, r_S and r_B are the radii of the colliding pair and *frac-avail* is the fraction of the surface area of the particle that is active for binding. This is the fraction of collisions with the correct alignment of ligand and receptor to allow binding to take place. For the free system this fraction is nearly one, whereas for the quantum dot system the fraction is vastly smaller than one (see Fig. 10). The *frac-avail* factor is calculated using the follow relation:

$$frac-avail = \prod_{i=1}^{particles} \left(n_{sites} \times \frac{r_{site}^2}{r_{particle}^2} \right)_i, \tag{18}$$

where n_{sites} is the number of binding sites per particle, r_{site} and $r_{particle}$ are the radii of the binding site and particle, respectively. The product is over the two particles involved in the collision; either QD_S-QD_B or streptavidin-biotin. Two binding scenarios are presented in Fig. 10, which depicts a cartoon of the collisions. In the cartoon, the fraction of quantum dot surface area available for binding is represented by small circles. These circles reflect the footprint of the

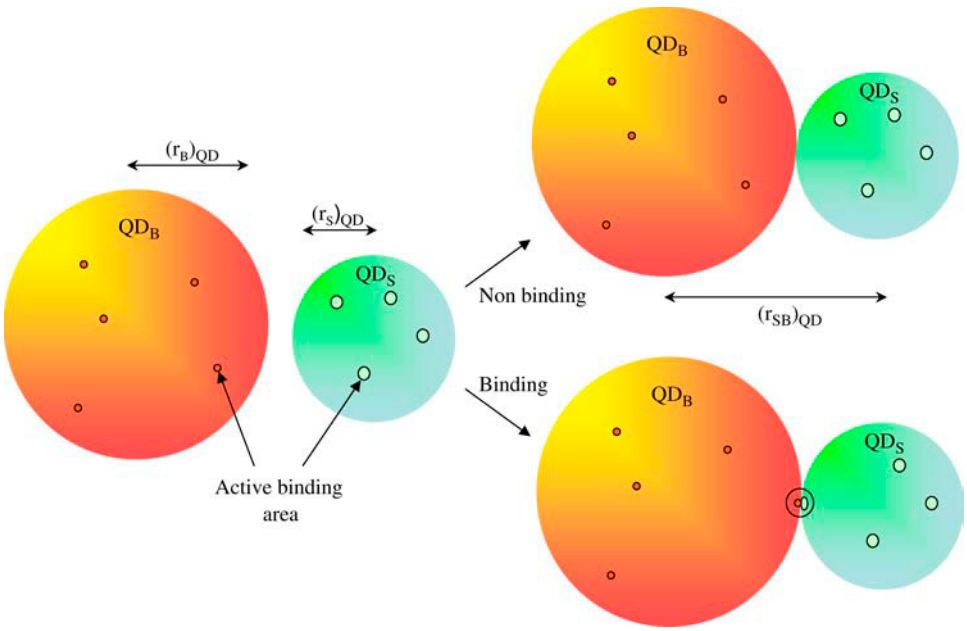

FIGURE 10 A cartoon of the relative probability of binding per QD_S-QD_B collision. The active binding areas on the quantum dots are drawn approximately to scale, as is the relative radii of the fully functionalized dots. A binding collision occurs when the active areas on the two dots overlap. This model is used to estimate the relative on-rate constants for free biotin and streptavidin versus QD_S-QD_B. See the text for details.

streptavidin binding site and of biotin on the quantum dot surface. In one case a collision between QD_S and QD_B results in binding; in the other, it does not.

The ratio from Eq. 18 was calculated using the crystallographic data (34,35) for the streptavidin binding site radius (0.5 nm), streptavidin radius (2.5 nm), and biotin radius (0.3 nm) and the radii of QD_S and QD_B from this work, (8 and 14 nm, respectively). Then using Eq. 17, a value of ~2200 was calculated for A_{free}/A_{QD}. The ratio of on-rate constants (free/QD) observed is 30,000. This value is calculated from the ratio $(k_{off}/K_d)_{free}/(k_{off}/K_d)_{QD}$. Therefore, although this approach moves toward the difference in k_{on}, it does not account for the entire difference. The difference between the estimated and measured rate coefficient ratios could result from rotational and orientational constraints for the quantum dot bound system, not accounted for in our simple model. Also, there may be a greater activation barrier to binding for the quantum dot system. The solvation shell around the quantum dots could be more extensive and require greater energy to rearrange during QD_S-QD_B binding than is required for binding of the native system. Further effects of fluorescence label size and chemistry on the dissociation constant and kinetics for streptavidin-biotin interactions are currently under investigation, but are beyond the scope of this study.

CONCLUSION

We have shown that it is possible to obtain relevant binding information for ligand-receptor systems that are bound to quantum dot nanocrystals. These assays are simple and easy to perform, making them ideal for future automation. In addition, the derived expression for P_A can be simply extracted from the auto and cross-correlation data and is independent of the excitation volume. The present assay allows for the full characterization of binding at low ligand concentrations, which are not achievable using other fluorescent assays. Moreover, it was possible to assess the degree to which binding to quantum dots perturbs the function of streptavidin. Based on the measured K_d and off-rate for unbinding, it appears that binding pocket of streptavidin is not significantly altered. Therefore, it was possible to attribute the lower value of K_d for the quantum dot system to changes in both the dissociation rate coefficient, k_{off}, and the association rate coefficient, k_{on}. Thus, a smaller K_d is related to the smaller probability of binding per QD_S-QD_B collision and the faster dissociation rate of the QD_S-QD_B system compared with that for free streptavidin-biotin.

APPENDIX: DERIVATION OF INTEGRATED RATE EQUATIONS FOR COMPETITION ASSAYS

If we consider the simplifying scenario of a 1:1 pair, QD_S:QD_B, in equilibrium with the free quantum dots, QD_S and QD_B, we can write the following equilibrium equation:

$$QD_S : QD_B \underset{k_{on}}{\overset{k_{off}}{\leftrightarrow}} QD_S + QD_B. \tag{A1}$$

Adding free d-biotin to this system can be approximated as a perturbation that removes free QD_S, thus promoting more dissociation of QD_S:QD_B to restore equilibrium. The differential rate law for this is:

$$\frac{dC_{SB}}{dt} = -k_{off}C_{SB} + k_{on}C_SC_B. \tag{A2}$$

If we make the approximation that C_B is constant, the differential rate law above can be rewritten:

$$\begin{aligned}\frac{dC_{SB}}{dt} &= -k_{off}C_{SB} + k'(C_{SB})_0 - k'C_{SB}\\ &= -(k_{off} + k')C_{SB} + k'(C_{SB})_0,\end{aligned} \tag{A3}$$

where $k' = k_{on}C_B$. This differential rate equation can be integrated giving:

$$C_{SB}(t) = (C_{SB})_0\frac{k_{off}}{k_{off} + k'}\left[\frac{k'}{k_{off}} + e^{-(k_{off} + k')t}\right]. \tag{A4}$$

Dividing both sides by $C_{SB} + C_S$ changes Eq. A4 to be relative to fractional occupancy, P_A:

$$P_A(t) = (P_A)_0\frac{k_{off}}{k_{off} + k'}\left[\frac{k'}{k_{off}} + e^{-(k_{off} + k')t}\right]. \tag{A5}$$

Because we can measure both $(P_A)_0$ and $(P_A)_\infty$, we can rewrite k' in terms of k_{off} by setting the equation above to the values at $t = \infty$ and solving for k':

$$k' = k_{off}\frac{(P_A)_\infty}{(P_A)_0 - (P_A)_\infty} = k_{off}\,\Delta P_A. \tag{A6}$$

Substituting this result into Eq. A5 and rearranging gives the final result:

$$\frac{P_A(t)}{(P_A)_0} = \frac{1}{1 + \Delta P_A}[\Delta P_A + e^{-k_{off}(1 + \Delta P_A)t}]. \tag{A7}$$

This is the equation used to model the decline in fractional occupancy after the addition of free d-biotin. It has only one adjustable parameter, k_{off}, which represents the rate constant of QD_S:QD_B unbinding.

The kinetics representing an increase in P_A observed for the dissociation of QD_S:dB are more complex. Here, we have to consider two reactions:

$$QD_S : dB \underset{k'_{on}}{\overset{k'_{off}}{\leftrightarrow}} QD_S + dB \tag{A8}$$

$$QD_S + QD_B \underset{k_{off}}{\overset{k_{on}}{\leftrightarrow}} QD_S : QD_B. \tag{A9}$$

If we assume the free QD_S is rapidly consumed by the free QD_B, then the reverse reaction in equation can be neglected. Therefore, the forward reaction of A8 is the rate-limiting step. We can then set up the differential rate equations for QD_S:dB, Q_S and QD_S:QD_B.

$$\frac{dC_{SdB}}{dt} = -k'_{off}\,C_{SdB} \tag{A10}$$

$$\frac{dC_S}{dt} = k'_{off}C_{SdB} - k_{on}C_SC_B + k_{off}C_{SB} \tag{A11}$$

$$\frac{dC_{SB}}{dt} = k_{on}\,C_S\,C_B - k_{off}C_{SB}. \tag{A12}$$

Under these conditions, the loss of QD_S:dB will follow the standard exponential decay. If we assume that the steady-state approximation holds

for Eq. A12, then we can solve for C_S and substitute the result for the steady-state approximation for the loss of QD_S:dB into the mass balance equation:

$$C_{SB} = (C_{SdB})_0 - C_{SdB} - C_S, \tag{A13}$$

to yield

$$C_{SB} = \frac{(C_{SdB})_0}{1 + \dfrac{k_{off}}{k_{on}C_B}}\left[1 - \left(1 - \frac{k'_{off}}{k_{on}C_B}\right)e^{-k'_{off}t}\right]. \tag{A14}$$

Recognizing that $(C_{SdB})_0$ equals the total available Q_S (i.e., $P_A = C_{SB}/(C_{SdB})_0$) and allowing for an excess of the competitor, QD_B, such that C_B is approximately constant (i.e., $k' = k_{on}C_B$), Eq. A14 can be rewritten:

$$P_A(t) = \frac{k'}{k' + k_{off}}\left[1 - \left(1 - \frac{k'_{off}}{k'}\right)e^{-k'_{off}t}\right]. \tag{A15}$$

SUPPLEMENTARY MATERIAL

An online supplement to this article can be found by visiting BJ Online at http://www.biophysj.org.

The authors are indebted to Professor David Armstrong (Calgary) and Professor Jolyon Jesty (SUNY, Stony Brook) for helpful discussions on kinetics.

Funding for this project was made possible by the Natural Sciences and Engineering Research Council of Canada (AGENO and CRD programs), AstraZeneca, and the Canadian Institute for Photonics Innovation. J.L.S. is grateful for a graduate scholarship from the Alberta Ingenuity Fund.

REFERENCES

1. Fang, Y., A. G. Frutos, and J. Lahiri. 2002. Membrane protein microarrays. *J. Am. Chem. Soc.* 124:2394–2395.
2. Schwille, P. 2001. Fluorescence correlation spectroscopy and its potential for intracellular applications. *Cell Biochem. Biophys.* 34: 383–408.
3. Schwille, P. 2000. Cross-correlation analysis in FCS. *In* Fluorescence Correlation Spectroscopy Theory and Applications. R. Rigler and E. S. Elson, editors. Springer, New York. 360–378
4. Wohland, T., K. Friedrich, R. Hovius, and H. Vogel. 1999. Study of ligand-receptor interactions by fluorescence correlation spectroscopy with different fluorophores: evidence that the homopentameric 5-hydroxytryptamine type ^{3}As receptor binds only one ligand. *Biochemistry.* 38:8671–8681.
5. Briddon, S. J., R. J. Middleton, A. S. Yates, M. W. George, B. Kellam, and S. J. Hill. 2004. Applications of fluorescence correlation spectroscopy to the measurement of agonist binding to a G-protein coupled receptor at the single cell level. *Faraday Discuss.* 126: 197–207.
6. Briddon, S. J., R. J. Middleton, Y. Cordeaux, F. M. Falvin, J. A. Weinstein, M. W. George, B. Kellam, and S. J. Hill. 2004. Quantitative analysis of the formation and diffusion of A_1-adenosine receptor antagonist complexes in single living cells. *Proc. Natl. Acad. Sci. USA.* 101:4673–4678.
7. Zemanova, L., A. Schenk, N. Hunt, G. U. Nienhaus, and R. Heiker. 2004. Endothelin receptor in virus-like particles; ligand binding observed by fluorescence fluctuation spectroscopy. *Biochemistry.* 43:9021–9028.
8. Heinze, K. G., A. Koltermann, and P. Schwille. 2000. Simultaneous two-photon excitation of distinct labels for dual: color fluorescence crosscorrelation analysis. *Proc. Natl. Acad. Sci. USA.* 97:10377–10382.
9. Berland, K. M., P. T. So, and E. Gratton. 1995. Two-photon fluorescence correlation spectroscopy: method and application to the intracellular environment. *Biophys. J.* 68:694–701.
10. Merkle, D., S. P. Lees-Miller, and D. T. Cramb. 2004. Lipoplex structure and dynamics examined using two-photon fluorescence cross-correlation spectroscopy. *Biochemistry.* 43:7263–7272.
11. Swift, J. L., A. Carnini, T. E. S. Dahms, and D. T. Cramb. 2004. Anesthetic-enhanced membrane fusion examined using two-photon fluorescence cross-correlation spectroscopy. I. *Phys. Chem. B.* 108: 11133–11138.
12. Hwang, L. C., and T. Wohland. 2004. Dual-color fluorescence cross correlation spectroscopy using single laser wavelength excitation. *ChemPhysChem.* 5:549–551.
13. Chan, W. C. W., D. J. Maxwell, X. Gao, R. E. Bailey, M. Han, and S. Nie. 2002. Luminescent quantum dots for multiplexed biological detection and imaging. *Curr. Opin. Biotechnol.* 13:40–46.
14. Larson, D. R., W. R. Zipfel, R. M. Williams, S. W. Clark, M. P. Bruchez, F. W. Wise, and W. W. Webb. 2003. Water soluble quantum dots for multiphoton fluorescence imaging *in vivo*. *Science.* 300: 1434–1437.
15. Tran, P. T., G. P. Anderson, J. M. Mauro, and H. Mattoussi. 2002. Use of luminescent CdSe-ZnS nanocrystal bioconjugates in quantum dot-based nanosensors. *Phys. Status Solidi. B.* 229:427–432.
16. Schroeder, A., H. Weller, R. Eritja, W. E. Ford, and J. M. Wessels. 2002. Biofunctionalization of silica-coated CdTe and gold nanocrystals. *Nano Lett.* 2:1363–1367.
17. Niemeyer, C. M. 2001. Nanoparticles, proteins, and nucleic acids: biotechnology meets materials science. *Angew. Chem. Int. Ed. Engl.* 40:4128–4158.
18. Bruchez, M., Jr., and M. Maronne. 1998. Semiconductor nanocrystals as fluorescent biological labels. *Science.* 281:2013–2017.
19. Dubertret, B., P. Skourides, D. J. Norris, V. Noireaux, A. H. Brivanlou, and A. Libchaber. 2002. In vivo imaging of quantum dots encapsulated in phospholipid micelles. *Science.* 298:1759–1763.
20. Pathak, S., S. K. Choi, N. Arnheim, and M. E. Thompson. 2001. Hydroxylated quantum dots as luminescent probes for in situ hybridization. *J. Am. Chem. Soc.* 123:4103–4104.
21. Akerman, M. E., W. C. W. Chan, P. Laakkonen, S. N. Bhatia, and E. Ruoslahti. 2002. Nanocrystal targeting *in vivo*. *Proc. Natl. Acad. Sci. USA.* 99:12617–12621.
22. Mitchell, G. P., C. A. Mirkin, and R. L. Letsinger. 1999. Programmed assembly of DNA functionalized quantum dots. *J. Am. Chem. Soc.* 121:8122–8123.
23. Ispasoiu, R. G., Y. Jin, J. Lee, F. Papadimitrakopoulos, and T. Goodson. 2002. Two-photon absorption and photon-number squeezing with CdSe nanocrystals. *Nano Lett.* 2:127–130.
24. Weber, P. C., D. H. Ohlendorf, J. J. Wendoloski, and F. R. Salemme. 1998. Structural origins of high-affinity biotin binding to streptavidin. *Science.* 234:85–89.
25. Schwartz, B. L., J. E. Bruce, G. A. Anderson, S. A. Hofstadler, A. L. Rockwood, R. D. Smith, A. Chilkoti, and P. S. Stayton. 1995. Dissociation of tetrameric ions of non-covalent streptavidin complexes formed by electrospray ionization. *J. Am. Soc. Mass Spectrom.* 6: 459–465.
26. Wiess, J. 1997. The Hill equation revisited: uses and misuses. *FASEB J.* 11:835–841.
27. Cornish-Bowden, A., and D. E. Koshland. 1975. Diagnostic uses of Hill plots. *J. Mol. Biol.* 95:201–212.
28. Michalet, X., F. Pinaud, L. Bentolila, J. Tsay, S. Doose, J. Li, G. Sundaresan, A. Wu, S. Gambhir, and S. Weiss. 2005. Quantum dots for live cells, in vivo imaging, and diagnostics. *Science.* 307:538–544.

29. Baudendistel, N., G. Muller, W. Waldeck, P. Angel, and J. Langowski. 2005. Two-hybrid fluorescence cross-correlation spectroscopy detects protein-protein interactions in vivo. *ChemPhysChem*. 6:984–990.

30. Eggeling, C., P. Kask, D. Winkler, and S. Jager. 2005. Rapid analysis of Forster resonance energy transfer by two-color global fluorescence correlation spectroscopy: trypsin proteinase reaction. *Biophys. J*. 89: 605–618.

31. Pelton, M., D. G. Grier, and P. Guyot-Sionnest. 2004. Characterizing quantum-dot blinking using noise power spectra. *Appl. Phys. Lett*. 85:819–821.

32. Hohng, S., and T. Ha. 2004. Near-complete suppression of quantum dot blinking in ambient conditions. *J. Am. Chem. Soc*. 126:1324–1325.

33. Huang, S. C., M. D. Stump, R. Weiss, and K. D. Caldwell. 1996. Binding of biotinylated DNA to streptavidin coated polystyrene latex: effects of chain length and particle size. *Anal. Biochem*. 237:115–122.

34. Hendrickson, W. A., A. Pahler, J. L. Smith, Y. Satow, E. A. Merritt, and R. P. Phizackerley. 1989. Crystal structure of core streptavidin determined from multiwavelength anomalous diffraction of synchatron radiation. *Proc. Natl. Acad. Sci. USA*. 86:2190–2194.

35. Chilkoti, A., and P. S. Stayton. 1995. Molecular origins of the slow streptavidin-biotin dissociation kinetics. *J. Am. Chem. Soc*. 117:10622–10628.